Crystallization of amorphous alloy during isothermal annealing: a molecular dynamics study

2005 J. Phys.: Condens. Matter 17 1493

(http://iopscience.iop.org/0953-8984/17/10/006)

INSTITUTE OF PHYSICS PUBLISHING JOURNAL OF PHYSICS: CONDENSED MATTER

J. Phys.: Condens. Matter **17** (2005) 1493–1504 doi:10.1088/0953-8984/17/10/006

Crystallization of amorphous alloy during isothermal annealing: a molecular dynamics study

Q X Pei[1], **C Lu and H P Lee**

Institute of High Performance Computing, 1 Science Park Road, Singapore 117528, Singapore

E-mail: peiqx@ihpc.a-star.edu.sg

Received 2 November 2004, in final form 19 January 2005
Published 25 February 2005
Online at stacks.iop.org/JPhysCM/17/1493

Abstract

The crystallization process of a Ti–Al amorphous alloy during isothermal annealing was studied with molecular dynamics simulations. The structural development and phase transformation were analysed based on the variations of the internal energy, cell volume, radial distribution function, bond pairs, and atomic configuration. The crystal nucleation, grain growth, and grain coarsening during the crystallization process were studied. The three-stage feature of the crystallization process was identified. The simulation results also show that there are transformations from a metastable crystal phase to a more stable crystal phase during the crystallization.

(Some figures in this article are in colour only in the electronic version)

1. Introduction

Crystallization of amorphous alloys has attracted increasing research interest in recent years, since it provides a way to fabricate nanostructured materials which have superior mechanical and unique physical properties [1–3]. Amorphous alloys used for the crystallization can be prepared through various non-equilibrium processes such as rapid solidification, physical vapour deposition, and mechanical alloying [4]. Because the amorphous structure is in a thermodynamically metastable state, it will undergo rearrangement and transform into crystalline structure during crystallization process. In experiments, crystallization is usually realized by isothermal annealing, in which the amorphous sample is maintained at a relative high temperature (higher than the crystallization temperature of the alloy) to induce crystallization [3, 5].

Molecular dynamics (MD) simulation is a very useful tool in materials research and has been widely used in studying the crystallization and glass formation processes of alloys during rapid solidification [6–10] to provide an atomic description of the structural development in

[1] Author to whom any correspondence should be addressed.

these processes. However, little work has been done to study the crystallization process of amorphous alloys during isothermal annealing and the associated crystal nucleation, grain growth and coarsening with MD simulation. The crystallization process of amorphous alloys during isothermal annealing is very complex; it usually involves nucleation and growth [3, 5], and phase transformation from metastable phases to stable phases [11]. It is therefore of interest to study this process with MD simulation.

In this paper, MD simulations are used to study the crystallization process of amorphous Ti–25% Al alloy during isothermal annealing, in order to get an atomic description of the crystallization process and to analyse the nucleation and grain growth process. Ti–Al alloys are attractive materials for aerospace and high temperature applications because of their special properties such as low density, high specific strength, high temperature strength, good oxidation and corrosion resistance. Another important reason to choose Ti–25% Al for this study is that this alloy has very strong crystal-forming ability, and thus it is possible for the amorphous structure to become crystallized within the nano-second timescale in the MD simulation.

2. Simulation method and conditions

The constant-pressure and constant-temperature molecular dynamics (NPT ensemble) was used in the simulation. The total number of atoms in the simulation system is 13 824, with the number of Ti atoms being 10 368 and the number of Al atoms being 3456, which corresponds to the composition of Ti–25% Al. The simulation was carried out in a box with periodic boundary conditions representing bulk volume and eliminating surface effect. The equations of motion were solved using a fourth-order Gear predictor–corrector algorithm with a time step $\Delta t = 5.0$ fs.

The amorphous Ti–Al alloys for the crystallization study were first prepared using the MD simulation by quenching the liquid Ti–Al alloys from 2000 K to room temperature (300 K) at a very high cooling rate of 100 K ps^{-1}. For Ti–25% Al, the amorphous structure is very difficult to obtain experimentally. However, it can be easily obtained in the MD simulation, in which the cooling rate can be extremely high.

The obtained amorphous structure in the rapid solidification of the MD simulation was confirmed by the atomic configuration and the radial distribution function of the structure. The crystallization process of the amorphous structure is simulated under isothermal annealing conditions with the annealing temperatures ranging from 500 to 700 K, which are below the glass transition temperature of about 800 K for Ti–25% Al [10] to make sure that the crystallization will start from the amorphous state, not the supercooled liquid state.

It should be noted that the constant pressure conditions are used in the MD simulations to allow the MD cell to change its volume in response to the imbalance between the internal and external applied pressure. In our pressure control scheme, only the cell lengths can change orthorhombically in x, y, and z directions, while the cell angles cannot change. Although the shape change of the MD cell was not allowed, we could still obtain quite good results of the phase transition in our simulations. This is because we used a large system with 13 824 atoms in the MD cell, which makes the effect of the cell shape restriction on the phase transition less important compared to a small system with a few hundred atoms. On the other hand, it was also reported [12] that the Rarrinello–Rahman method of pressure control which allows shape change often resulted in collective transformation across the whole simulation cell instead of the process via nucleation and growth as expected in the real system.

The inter-atomic potential plays a key role in MD simulation. The embedded atom method (EAM) potential [13] was used in our simulations to consider the many-body effect due to metallic bonding. For the EAM potential, the total atomic potential energy of a system is

expressed as

$$E_{\mathrm{tot}} = \tfrac{1}{2}\sum_{i,j}\Phi_{ij}(r_{ij}) + \sum_{i}F_i(\bar{\rho}_i) \tag{1}$$

where Φ_{ij} is the pair-interaction energy between atoms i and j, and F_i is the embedding energy of atom i. $\bar{\rho}_i$ is the host electron density at site i induced by all other atoms in the system, which is given by

$$\bar{\rho}_i = \sum_{j\neq i}\rho_j(r_{ij}). \tag{2}$$

Since the EAM was first proposed by Daw and Baskes about 20 years ago [14], the EAM potentials for some pure metals and a very limited number of binary alloys have been constructed by fitting to experimental data. However, recent studies [15, 16] have shown that the incorporation of *ab initio* data into the construction of interatomic potentials can significantly enhance their ability to mimic the interatomic interactions. In this paper, we use the EAM potential for Ti–Al alloy that was recently developed by Zope and Mishin [17] by fitting to a large database of both experimental and *ab initio* data.

3. Structural analysis methods

During isothermal annealing, variations of the internal energy, cell volume, and atomic configuration are monitored in the MD simulations to analyse the crystallization process, because these parameters are closely related to the structural rearrangement of the atomic system. The internal energy is the potential energy of the atoms, which becomes lower as the atoms move closer to the equilibrium positions. As the atoms rearrange from the disordered amorphous state to the well ordered crystalline state, the cell volume becomes smaller. In addition, the radial distribution function and the pair analysis technique are also used to analyse the structural change during crystallization.

3.1. Radial distribution function

The radial distribution function (RDF), or $g(r)$, is a structural parameter to quantify the average structure of the molecular system. The RDF shows the structural characteristics of the atomic system, such as the ordering degree of the atoms. It has been widely used to describe the structural change between liquid, amorphous, and crystalline structures. The RDF is defined as the probability of finding an atom a distance r from another atom, and is calculated by [18]

$$g(r) = \frac{1}{\rho^2}\left\langle\sum_{i}\sum_{j\neq i}\delta(r + r_i - r_j)\right\rangle \tag{3}$$

where the angle brackets are used to denote a spherical average as well as the usual configurational average. In the code, $g(r)$ is evaluated from a histogram of pair distances accumulated during a simulation run. With the notation that N is the total number of atoms, b is the number of histogram bins, δr is the width of the bin, $n(b)$ is the accumulated number per bin, and m is the number of steps when binning was carried out, then

$$g(r + \delta r/2) = \frac{3n(b)}{4\pi\rho N m[(r+\delta r)^3 - r^3]}. \tag{4}$$

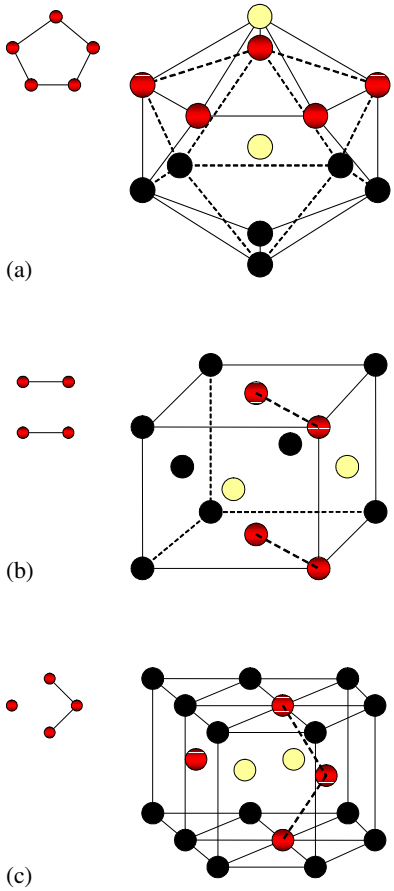

Figure 1. Three typical bond pairs: (a) pair 1551; (b) pair 1421; (c) pair 1422.

3.2. Pair analysis technique

The pair analysis technique was mainly developed by Honeycutt and Andersen [19] to study the melting and freezing of atoms clusters and it has been used to monitor the structural change during rapid solidification process [8, 9].

In this technique, a pair of atoms is taken as a bond pair if their distance is smaller than a specified cut-off distance, which is chosen to be equal to the position of the first minimum in the corresponding radial distribution function. Honeycutt and Andersen used a sequence of four integers i, j, k, and l to show various atom pairs. For any pair of atoms A–B (root pair), if the two atoms form a bond, $i = 1$; otherwise, $i = 2$. The second integer j represents the number of common atoms, which form bonds with both atom A and atom B. The third integer k represents the number of bonds formed among the common atoms. The fourth integer l represents the way which the bonds formed among the common atoms. If these bonds link in turn, $l = 1$; otherwise $l = 2$. For example, the 1551 atom pair means that the two root pair atoms form a bond and they have five bonded common atoms that form five bonds among the common atoms. Figure 1 shows three typical bond pairs in the atom system.

The various atom pairs characterize different local structures. The 1551 pair forms a pentagon type of near-neighbour contact, and so the number of 1551 pairs is a direct

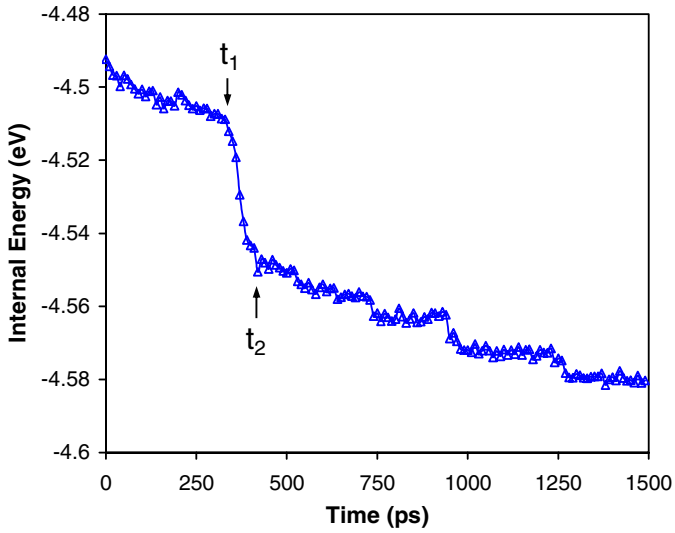

Figure 2. Variation of internal energy during annealing at 700 K.

measurement of the degree of icosahedral ordering. The 1541 and 1431 pairs represent the icosahedral defect and fcc defect local structures. The 1551, 1541, and 1431 pairs are relatively numerous in liquid and amorphous state. The 1421 and 1422 pairs are found mostly in fcc-like and hcp-like local structures, while the 1441 and 1661 pairs are found greatly in bcc-like local structures. By analysing the variations of the atoms pairs, information on the structural change of the atomic system can be obtained.

4. Simulation results and discussion

Since the amorphous phase is thermodynamically unstable, the transformation to a more stable phase should occur when the annealing temperature is above the crystallization temperature. We now analyse the simulation results at the annealing temperature of 700 K.

Figure 2 shows the variation of the internal energy during annealing at 700 K. It can be seen from the curve that there are big drops of the internal energy, which means that the atoms move closer to the equilibrium positions, and the atomic system rearranges from the disordered amorphous state to the well ordered crystalline state, and thus the crystallization has happened in the simulation time period. It can also be seen that from the annealing start to t_1 (at 330 ps) the internal energy decreases slowly. However, from t_1 to t_2 (at 420 ps) the internal energy decreases very fast. After the time of t_2, the internal energy decreases slowly again. Similar curves are obtained for the cell volume during annealing, as shown in figure 3. It is interesting to see that the slopes for the different parts of the curves, i.e. at different time periods during annealing, show a big difference, which may represent different crystallization stages. From the annealing start to t_1, the internal energy and the cell volume show a slow drop. We define this period as the first stage of crystallization. From time t_1 to time t_2 there is a very sharp drop of the internal energy and cell volume, which is defined as the second stage of crystallization. From time t_2 to the simulation end (at 1500 ps), the internal energy and the cell volume show a slow drop again, which is defined as the third stage or final stage of crystallization.

During the annealing process, the first stage of crystallization may be interpreted as the structural relaxation and the nucleation of crystalline phases in the amorphous matrix.

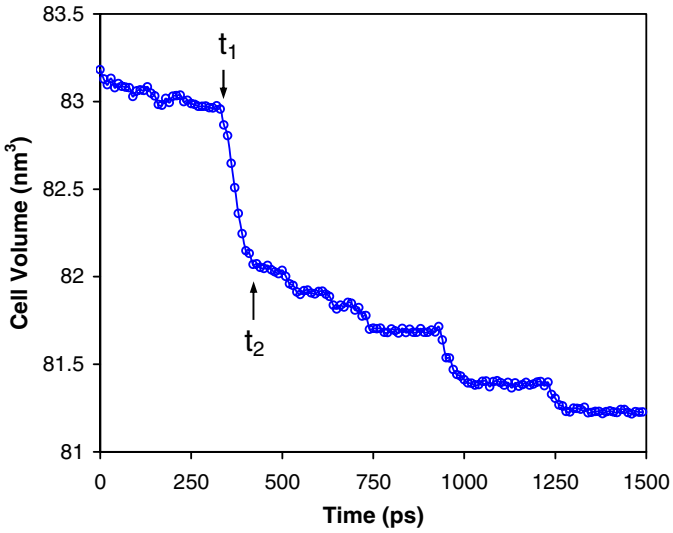

Figure 3. Variation of cell volume during annealing at 700 K.

The second stage of crystallization may be related to the fast growth of the crystalline phases, while the third stage (final stage) of crystallization may be related to the coarsening of the crystalline phases. The structural development during annealing and the three crystallization stages is further analysed with the RDF, pair analysis, and atomic configuration of the system.

Figure 4 shows the RDFs at different annealing times during crystallization at 700 K. The RDF can show whether the atoms are distributed in a more orderly or more disorderly way. It can be seen that the annealing process starts from the amorphous phase, which is because the RDF shows the well known feature of amorphous structure, that is, the splitting of the second peak. At the time of 330 ps, which is at the end of the first stage of crystallization, the split of the second peak becomes less obvious due to the nucleation of crystal phase. When the annealing time reaches 420 ps, which is at the end of the second stage of crystallization, the RDFs show the feature of crystal structure due to the rapid growth of the crystal grains. During the third stage of crystallization, the peaks in the RDFs at times of 700, 1000, and 1500 ps become sharper. This implies that the crystallized phase undergoes coarsening with further thermal annealing in this stage, which results in fewer grain boundaries and more obvious crystal features. The above changes in RDF clearly show that there exists a transformation from the disordered amorphous structure to the ordered crystalline structure during the crystallization process. However, the RDF can only provide the overall description of the crystallization process, and cannot provide an accurate identification of the structural change.

To identify the structural change during the crystallization process more clearly, a quantitative evaluation of atomic structure is desired. For this purpose, the local structure analysis technique, pair analysis, has been used in the study. In pair analysis, the bond pairs 1421, 1422, 1441, and 1661 exist mostly in different crystallized structures, while the bond pairs 1551, 1541, and 1431 exist mainly in amorphous structure. Therefore, the pairs 1421, 1422, 1441, and 1661 are called crystal pairs, while the pairs 1551, 1541, and 1431 are called amorphous pairs. The variations of the amorphous pairs and crystal pairs in the annealing process are shown in figures 5(a) and (b) respectively. It can be seen from figure 5(a) that the numbers of the three amorphous pairs decrease during annealing, which means that the amorphous phase transforms into crystal phase. Besides, figure 5(b) shows that the crystal

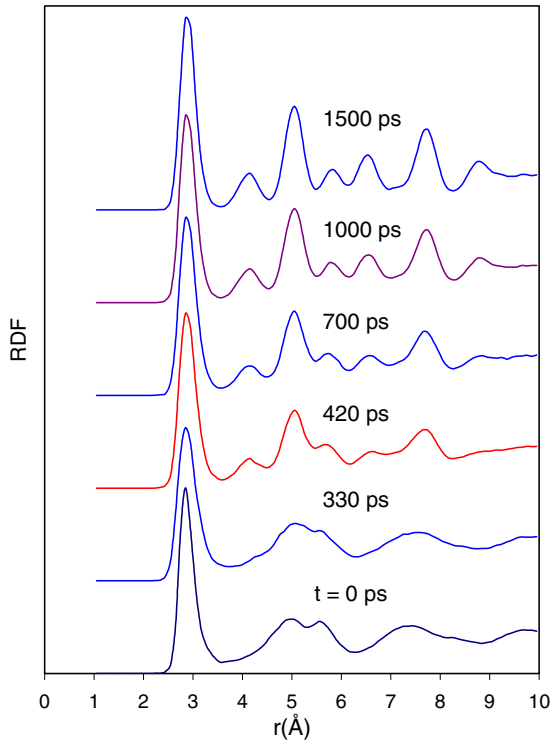

Figure 4. The radial distribution functions (RDFs) at different annealing times during the crystallization process.

pair 1422 decreases, while the crystal pair 1421 increases, which indicates that some hcp-like local structures have transformed into fcc-like local structures during the crystallization process. The transformation from metastable crystal phase into more stable crystal phase has often been observed in crystallization experiments [11]. Our results clearly show that such transformation did happen in the MD simulation.

Figure 6 shows the sum of all the crystal pairs and the sum of all the amorphous pairs as a function of annealing time. The curves clearly show that the total number of the crystal pairs increases, while the total number of the amorphous pairs decreases correspondingly, which shows that the crystal phase forms at the expense of the amorphous phase. Besides, the three crystallization stages identified in figures 2 and 3 can be further confirmed by the curves. The increasing number of crystal pairs and the decreasing number of amorphous pairs in the first stage of crystallization (from annealing start to t_1) clearly show that the crystal phases nucleate in the amorphous matrix. In the second stage of crystallization (from t_1 to t_2) the rapid increasing of the crystal pairs and the sharp drop of the amorphous pairs in the short time period show that the crystal grains grow very fast in this stage. In the third stage of crystallization (from t_2 to the simulation end), the slow increasing of crystal pairs implies the grain coarsening after growth.

From figure 6 it can be seen that crystal pairs exist in the as-quenched amorphous structure, which means that there are crystal embryos in the amorphous matrix. During the nucleation phase, some of the crystal embryos grow and act as crystal nuclei. At time t_1, the crystal nuclei have reached a critical size and then they begin to grow rapidly. By using the pair analysis

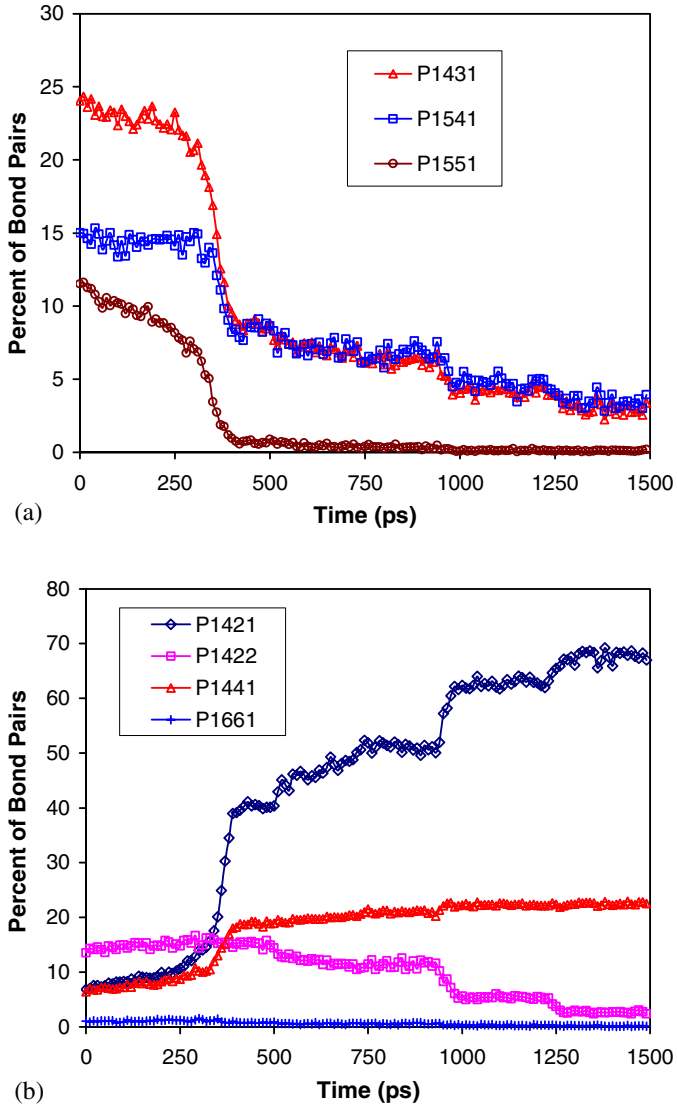

Figure 5. Variations of various bond pairs during annealing: (a) amorphous pairs; (b) crystal pairs.

technique, the critical nucleus size is estimated to be 30–50 atoms. Figure 7 shows a critical nucleus at time t_1. The nucleated phases during the crystallization process are mainly solid solution, as the crystallization time is too short for the atoms to diffuse long distances to form the perfect crystal structure of TiAl or Ti_3Al.

The structural development during the crystallization process is further explored with the computer visualization of the atom system. Figures 8(a)–(f) show snapshots of atomic configuration during crystallization at 700 K. Figure 8(a) shows the atomic configuration of the as-quenched amorphous alloy at the start of the crystallization. This image represents a typical amorphous structure, in which the atoms are distributed in a disordered way. Figure 8(b) shows the atomic configuration at the end of the first stage crystallization (at 330 ps). It can be

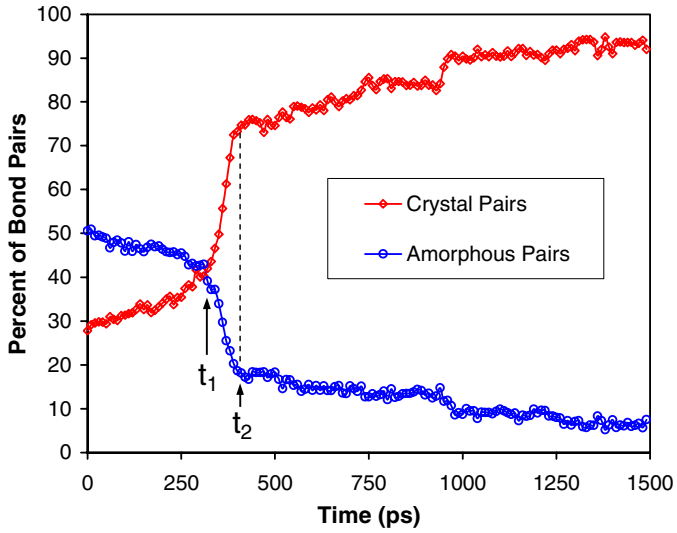

Figure 6. Variations of the total numbers of crystal pairs and the total number of amorphous pairs during annealing.

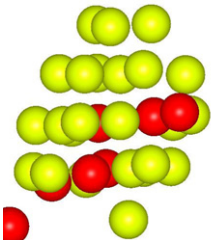

Figure 7. A critical crystal nucleus during crystallization in the MD simulation. The dark (red) balls are Al atoms.

observed from this image that some nuclei of ordered structure have formed in the matrix of the disordered structure, i.e. crystalline phases nucleate from the amorphous phase. Figure 8(c) shows the atomic configuration at the end of the second stage crystallization (at 420 ps), in which the ordered crystalline structure has been almost completely formed, i.e. the grains have grown. During the third stage of crystallization, the grain coarsening can be clearly observed from the atomic configurations in figures 8(d)–(f). Figure 8(f) shows the atomic configuration at the simulation end (at 1500 ps), in which the atoms show a well ordered crystalline structure after grain coarsening and structure relaxation.

The grain growth process is quite fast, taking about 90 ps, while the grain coarsening process is slower, taking more than 1000 ps. During the grain coarsening process, large grains grow by consuming smaller neighbouring grains through grain rotation and grain boundary migration.

The above results with the internal energy, cell volume, RDFs, bond pairs, and atomic configurations clearly show the structural development and phase transformation during the isothermal annealing. The structural development shows three distinct stages in the crystallization process. The first transition stage corresponds to the primary stage of crystallization, in which some degree of short-range ordering (crystal nuclei) occurs in the

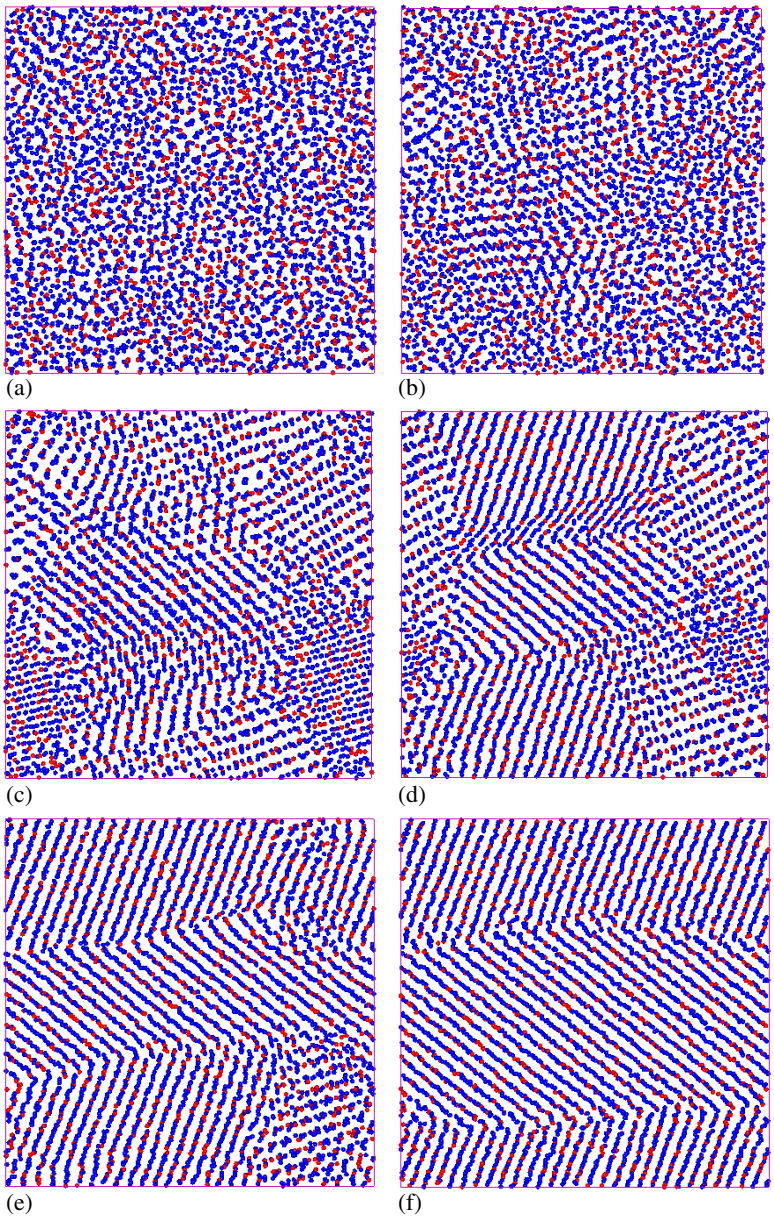

Figure 8. Snapshots of the atomic configuration during the crystallization process of Ti–25% Al alloy. (a) $t = 0$ ps; (b) $t = 330$ ps; (c) $t = 420$ ps; (d) $t = 700$ ps; (e) $t = 1000$ ps; (f) $t = 1500$ ps.

amorphous matrix. In the second transition stage, the crystal nuclei grow rapidly and almost all the amorphous structure transform into crystalline structure. In the final transition stage, the crystal grains undergo coarsening. This three-stage crystallization has been shown recently by Lu and Zhang [20] in their experiments on crystallizing amorphous $FeZr_2$ alloy, by means of electrical resistance measurement and the TEM observation. The three-stage transition may be considered as the general process in crystallizing amorphous alloys [5, 20], because

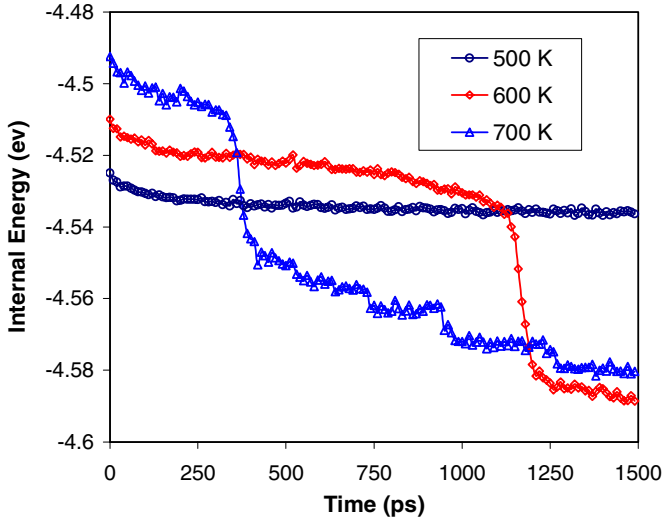

Figure 9. Variations of the internal energy during annealing for different annealing temperatures.

amorphous solids can be viewed as 'frozen melts' and thus their crystallization processes are analogous to the solidification processes of the melts, which consist of crystal nucleation and subsequent growth of the crystal nuclei.

It should be pointed out that the crystallization time in the MD simulation is much shorter than that in experiments. This is because the material used in the MD simulations is Ti–25% Al, which is very difficult to make amorphous in real experimental conditions, even by vapour deposition. Therefore, the amorphous Ti–25% Al has very strong crystallization ability and thus it can crystallize in the nanosecond timescale in the MD simulation.

The effect of the annealing temperature on the crystallization process was also investigated in the MD simulations. Figure 9 shows the variations of the internal energy at different annealing temperatures. For the simulation case with the annealing temperature of 500 K, the internal energy decreases very slowly. Moreover, there is no sharp energy drop and the total amount of energy drop is very small in the simulation. Therefore, at the annealing temperature of 500 K, there is only some structural relaxation and no crystallization happening in the simulation. For the simulation case with the annealing temperature of 600 K, the internal energy curve is similar to that of the 700 K case analysed above. Therefore, crystallization has happened at the annealing temperature of 600 K. In addition, its internal energy curve also shows that the crystallization process undergoes the three-stage transition similar to the case of 700 K. Besides, from the energy curves in figure 9, it can be seen that the higher the annealing temperature, the faster the crystallization process, which is consistent with experimental observations [11].

5. Summary and conclusions

Based on the EAM potential for the Ti–Al system that was recently developed by Zope and Mishin [17], MD simulations were performed to study the crystallization process of the Ti–25% Al amorphous alloy during isothermal annealing. The simulation results show that the transition from amorphous structure to crystal structure is a continuous process, associated with the sharp variations in the internal energy, cell volume, RDF, bond pairs, and atomic

configuration of the system. The analysis of the phase transition with these parameters can give us a clear picture of the crystallization process.

From the simulation results, the crystallization process was identified by three transition stages: (1) the nucleation of the crystals in the amorphous matrix; (2) the growth of the crystal nuclei; (3) the coarsening of the crystal grains. In addition, the transformation from a metastable crystal phase to a more stable crystal phase during the crystallization was also identified in the simulation. The simulation results also show that the higher the annealing temperature, the faster the crystallization process. These simulation results are consistent with experimental findings.

Acknowledgment

This work was supported by the Agency for Science, Technology and Research (A*Star), Singapore.

References

[1] Chow G M and Noskova N I (ed) 1998 *Nanostructured Materials: Science & Technology* (Dordrecht: Kluwer–Academic) p 143
[2] Lu K 1996 *Mater. Sci. Eng. Rep.* **16** 161
[3] Kulik T J 2001 *Non-Cryst. Solids* **287** 145
[4] Suryanarayana C (ed) 1999 *Non-Equilibrium Processing of Materials* (Amsterdam: Pergamon)
[5] Greer A L 1996 *Metall. Mater. Trans.* A **27** 549
[6] Carprion D and Schober H R 2002 *J. Chem. Phys.* **117** 7506
[7] Sheng H W, He J H and Ma E 2002 *Phys. Rev.* B **65** 184203
[8] Liu C S, Xia J, Zhu Z G and Sun D Y 2001 *J. Chem. Phys.* **114** 7506
[9] Li G X, Liang Y F, Zhu Z G and Liu C S 2003 *J. Phys.: Condens. Matter* **15** 2259
[10] Pei Q X, Lu C and Fu M W 2004 *J. Phys.: Condens. Matter* **16** 4203
[11] Abe T, Akiyama S and Onodera H 1994 *ISIJ Int.* **34** 429
[12] Zipoli F, Bernasconi M and Martonak R 2004 *Eur. Phys. J.* B **39** 41
[13] Daw M S, Foiles S M and Baskes M I 1993 *Mater. Sci. Rep.* **9** 251
[14] Daw M S and Baskes M J 1983 *Phys. Rev. Lett.* **50** 1285
[15] Baskes M J, Asta M and Srinivasan S G 2001 *Phil. Mag.* A **81** 991
[16] Belonoshko A B, Ahuja R, Eriksson O and Johansson B 2000 *Phys. Rev.* B **61** 3838
[17] Zope R R and Mishin Y 2003 *Phys. Rev.* B **68** 024102
[18] Hansen J P and McDonald I R 1986 *Theory of Simple Liquids* (London: Academic) p 455
[19] Honeycutt J D and Andersen H C 1987 *J. Phys. Chem.* **91** 4950
[20] Lu K and Zhang X H 2000 *Phil. Mag. Lett.* **80** 797